Giant Vesicles

DOI: 10.1002/anie.201208425

Hydrodynamically Driven Self-Assembly of Giant Vesicles of Metal Nanoparticles for Remote-Controlled Release**

*Jie He, Zengjiang Wei, Lei Wang, Zuleykhan Tomova, Taarika Babu, Chaoyang Wang, Xiaojun Han, John T. Fourkas, and Zhihong Nie**

Self-assembly of molecular amphiphiles (for example, surfactants or amphiphilic block copolymers (BCPs)) into vesicles mimics the construction of biological membranes composed of lipid bilayers.[1] These vesicles, namely liposomes or polymersomes, have received considerable attention owing to their appealing applications in drug delivery,[2] biosensing,[3] and catalysis.[4] The incorporation of inorganic nanoparticles (NPs) into vesicular membranes can endow them with advanced functionalities (for example, plasmonic, magnetic, and luminescent properties)[5] while preserving the well-established properties of organic components. The presence of NPs with inherent rigidity can also significantly extend the elastic modulus of vesicles, thus offering mechanical advantages over their organic counterparts.[6] Recently, polymer-tethered amphiphilic NPs have received considerable attention as a new class of nanoscale colloidal building blocks for fabricating functional materials.[5c–f,7] Resembling molecular amphiphiles, these materials merge the nature of polymers and inorganic NPs to organize into a wide range of nanostructures, including micelles, vesicles, wires, and tubules.[5c–f,7]

Giant vesicles having diameters of 1–100 μm are attractive for a variety of applications, including microreactors for chemical or biomimetic synthesis,[8] artificial biomembranes for mimicking live cells and modeling protocells,[9] and delivery vehicles for drugs or biomolecules.[10] The introduction of inorganic NPs in giant vesicles can have a significant impact on their properties and applications. Toyota et al. recently demonstrated that giant vesicles loaded with iron oxide NPs display a significant enhancement of contrast for magnetic resonance imaging of single cells.[10c] These vesicular contrast agents not only generate high signal levels comparable to microsized iron oxide particles, but also are easily cleared out as discrete nanoparticles after the dissociation of vesicles.

Current strategies for the self-assembly of vesicles from colloidal amphiphiles typically include solvent mixing, dialysis, and film rehydration methods that are commonly used for molecular self-assembly.[11] These methods show poor batch-to-batch reproducibility and limited control over the size of the vesicles (usually 50 to 500 nm).[11] Microfluidic approaches have demonstrated superior controllability in the self-assembly of lipids and amphiphilic BCPs.[11b,12] However, to date, there has been no report of a template-free approach to the high-throughput self-assembly of giant vesicles with controlled dimensions using inorganic NPs, especially polymer or BCP-tethered NPs.

Herein we report a simple yet robust microfluidic platform for the continuous self-assembly of polymer-tethered amphiphilic NPs into various structures with controlled size and morphology. This novel strategy uses hydrodynamic flow to control the kinetic aspects of the assembly process, thus achieving non-equilibrium structures. In contrast to conventional building blocks of molecular amphiphiles, the use of BCP-tethered amphiphilic NPs enables the reproducible generation of monodispersed giant vesicles comprising a monolayer of NPs in the membranes (Figure 1). These materials are unattainable by other current approaches. The size of giant vesicles can be tuned in the range of 500 nm to 2.0 μm by controlling the flow rates of each fluid. Of note, the self-assembly mechanism of our giant vesicles differs conceptually from the fabrication of conventional colloidosomes by using emulsions or double emulsions as templates.[13] Furthermore, the pathways of NP self-assembly can be selected to produce other types of nanostructures, such as micelles and disk-like structures comprising a monolayer of NPs (Figure 1b). This general approach is applicable to NPs with different shapes as well. Furthermore, we demonstrate the encapsulation of hydrophilic molecules in vesicles and the subsequent remote-controlled burst release of the payload using near infrared (NIR) irradiation.

PDMS-based microfluidic flow-focusing devices (MFFDs) were used to control the self-assembly of polymer-tethered NPs (Figure 1).[11b,12a–h] Gold nanorods (AuNRs)

[*] Dr. J. He, Z. Wei, L. Wang, Z. Tomova, T. Babu, Prof. Dr. J. T. Fourkas, Prof. Dr. Z. Nie
Department of Chemistry and Biochemistry
University of Maryland, College Park, MD 20742 (USA)
E-mail: znie@umd.edu
Z. Wei, Prof. Dr. C. Wang
Research Institute of Materials Science
South China University of Technology
Guangzhou 510640 (China)
L. Wang, Prof. Dr. X. Han
School of Chemical Engineering and Technology
Harbin Institute of Technology, Harbin 150001 (China)
Prof. Dr. J. T. Fourkas
Institute for Physical Science and Technology
University of Maryland, College Park, MD 20742 (USA)

[**] This work is supported by startup funds and the Research and Scholarship Award from the University of Maryland. We thank Dr. Wen-An Chiou for help with Cryo-TEM imaging. T.B. thanks the support of Arnold and Mabel Beckman Foundation. Z.W. thanks the support of the China Scholarship Council. We also acknowledge the support of the Maryland NanoCenter and its NispLab and FabLab. The NispLab is supported in part by the NSF as a MRSEC Shared Experimental Facilities.

Supporting information for this article is available on the WWW under http://dx.doi.org/10.1002/anie.201208425.

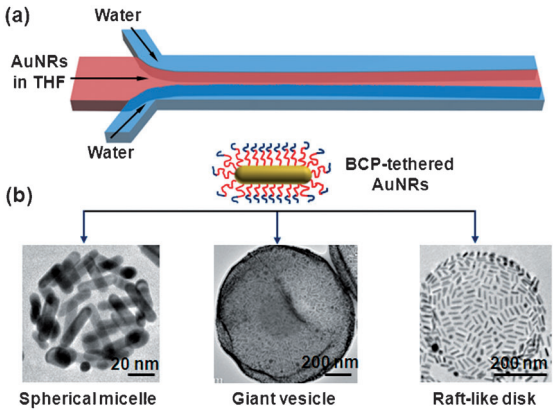

Figure 1. a) Hydrodynamic self-assembly of amphiphilic NPs tethered with BCPs using microfluidic flow-focusing devices (MFFDs). A THF solution of polymer-tethered NPs was focused by two water streams on the sides. b) TEM images of assemblies of PEO_{45}-*b*-PS_{211} tethered to AuNRs and obtained at different hydrodynamic conditions in MFFDs.

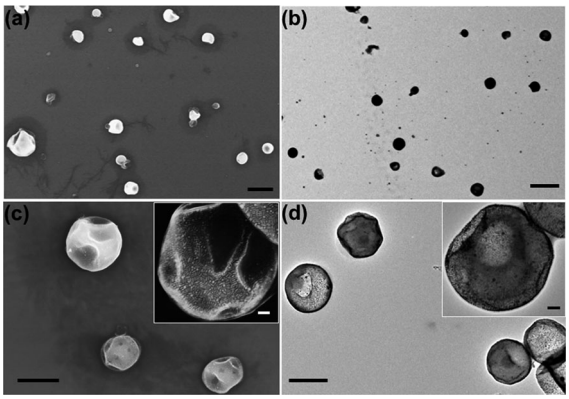

Figure 2. Representative SEM (a,c) and TEM (b,d) images of giant vesicles prepared at $Q_{THF} = 10\ \mu L\,min^{-1}$ and $Q_{H_2O} = 90\ \mu L\,min^{-1}$. The insets in (c,d) are high-magnification images of vesicles. Scale bars are 3 μm in (a,b), 1 μm in (c,d) and 100 nm in the insets of (c,d).

(40 nm in length and 10 nm in diameter) were chosen as a model system owing to their unique tunable plasmon absorption in the NIR region, and their resulting biomedical applications in drug delivery, imaging, and diagnosis.[14] The AuNRs were modified with amphiphilic linear BCPs of PEO_{45}-*b*-PS_{211} ($M_n = 23.9\ kg\,mol^{-1}$, PDI = 1.15) terminated with a thiol group at the PS end by ligand exchange in dimethylformamide. The thiol-terminated PEO_{45}-*b*-PS_{211} was synthesized by reversible addition fragmentation chain-transfer polymerization, followed by the reduction of dithioester groups.[5f] The self-assembly of BCP-tethered AuNRs was triggered by focusing a tetrahydrofuran (THF) solution of AuNRs (ca. $0.02\ mg\,mL^{-1}$) between two streams of water at a junction to enter a common outlet channel in the MFFD (Figure 1 a). Because of the low Reynolds number ($Re < 6$) in microchannels, the two miscible fluids formed a laminar flow with well-defined mixing between adjacent laminar streams. The diffusive boundaries between the miscible streams provide a precisely regulated environment for the rapid and continuous self-assembly of NPs. The self-assembly of BCP-tethered NPs is driven by amphiphilicity, as a result of the conformation change of BCP tethers on the surface of AuNRs.[5f] By varying the flow rates of each fluid, the microfluidic strategy allows for precise control of the width of the central stream as well as the diffusive mixing at the boundaries of streams, thus tuning the pathways of NP self-assembly.

Figure 2 shows representative electron micrographs of giant vesicles generated by MFFDs. Such giant vesicles are composed of a monolayer of AuNRs in the shell, with rods side-by-side aligned along the periphery of vesicles (for more images, see the Supporting Information). The formation of giant vesicles occurs within a specific window of hydrodynamic conditions, which are defined by the volume flow rates (Q) of THF and water streams. For example, at $Q_{THF} = 10\ \mu L\,min^{-1}$ and $Q_{H_2O} = 90\ \mu L\,min^{-1}$ (the total flow rate of two water streams that were operated at the same flow rate), giant vesicles with an average diameter of $1.28 \pm 0.4\ \mu m$ are produced (for optical images and more low-magnification SEM/TEM images, see the Supporting Information). The formation of rather monodispersed vesicles can be ascribed to the solely diffusive transport of solvents and NPs during the assembly process without the disturbance of hydrodynamic convection. The hollow interior of vesicles was confirmed by confocal fluorescence microscopy images (hydrophobic dyes were loaded in membranes of the vesicles) and multiphoton-absorption-induced luminescence (MAIL) images (Supporting Information).[15] In both cases, the luminescent images present typical ring-shaped patterns, indicating the hollow interior of vesicles. The hollow vesicular structures were also confirmed by the wrinkle features of the assemblies in SEM and TEM images, which are a result of the buckling and flattening of vesicular shells on the substrate during drying. We emphasize that the direct mixing of a solution of BCP tethered to AuNRs in THF with water at various adding speeds and the same final water content cannot generate the giant vesicles mentioned above, but rather can only form small clusters or small vesicles of AuNRs.[5f] This observation suggests that the appropriate kinetic control in channels plays a critical role in microfluidic-assisted NP self-assembly process. Note that the microfluidic approach is also applicable to assembling BCP-tethered spherical AuNPs (Supporting Information).

The microfluidic approach allows us to fine-tune the assembled structures by controlling the fluidic environment. The morphologies of assemblies are largely dependent on the flow-rate ratio, FRR, of the water phase to THF–AuNR phase, $FRR = Q_{H_2O}/Q_{THF}$. Figure 3 a maps the hydrodynamic effect on the morphologies of assembled NPs onto the ($\log Q_{H_2O}$, $\log Q_{THF}$) space. The product diagram outlines the hydrodynamic regions of NP assemblies with various morphologies including micelles, giant vesicles, and disks. When $FRR > 7.5$, that is, $Q_{THF} \ll Q_{H_2O}$, the central THF stream is strongly focused by two water streams, and is depleted rapidly in the downstream channel close to the junction. The amphiphilic AuNRs assembled into small micelles with diameter smaller than 100 nm in this high focusing region (rather than in the downstream channel). The resulting

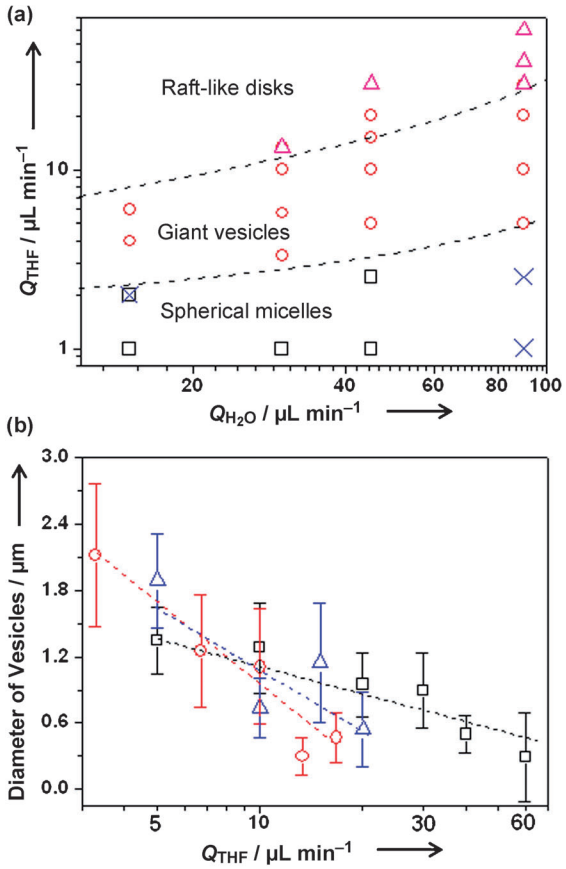

Figure 3. a) The product diagram of the self-assembly of polymer-tethered AuNRs in the [log Q_{THF}, log Q_{H_2O}] space: micelles (□), disks (△), giant vesicles (○), and no assemblies (×). b) The size of giant vesicles as a function of the flow rate of central THF phase at a fixed water flow rate: 90 µL min^{-1} (□), 45 µL min^{-1} (△), and 30 µL min^{-1} (○).

micelles are composed of randomly packed AuNRs. For example, at $Q_{THF} = 1$ µL min^{-1} and $Q_{H_2O} = 30$ µL min^{-1}, micelles of AuNRs with a diameter of 83.8 ± 23.9 nm are obtained (Supporting Information, Figure S11). When decreasing the FRR to $2.5 < FRR < 7.5$, the self-assembly of NPs undergoes a sharp transition from micelles to giant vesicles with diameter above 500 nm. In this case, a relatively wider center THF stream is focused to form a laminar flow with three side-by-side streams. The self-assembly of AuNRs mainly occurs at the boundary of the fluidic streams in the downstream region (rather than in the flow-focusing region), resulting in the formation of giant vesicles. With further decrease of FRR below 2.5, AuNRs assemble into disk-like micelles containing a single layer of AuNRs (Supporting Information, Figure S12). The disk-like structures can be considered as intermediate structures before their enclosure to form giant vesicles.[16] The formation of disk-like micelles was further confirmed using cryo-TEM (Supporting Information, Figure S13). The diameter of the disks is in the range of 300–500 nm. The spacing between NRs is 11.4 nm, which is slightly larger than that in giant vesicles owing to the swelling of polymers in a large fraction of THF.

It is noteworthy that the formation and morphological transition of assemblies are largely determined by the mixing time of the two streams (that is, the flow-rate ratio of two phases),[12c] rather than by the solvent compositions, as direct mixing cannot yield these nanostructures. Moreover, the assemblies are stable in solution or with the further addition of water, and the integral structures of giant vesicles are well-maintained after six months. AuNR assemblies with different morphologies in solution were also confirmed by measuring the surface plasmon resonance (SPR; Supporting Information, Figure S17). The organization of AuNRs significantly reduces the distance between neighboring NRs, leading to a clear red-shift (up to about 120 nm) in their SPR peak owing to plasmonic coupling between NRs.

Apart from control over the kinetic pathways of assembly, this microfluidic method enables simple control of the dimension of the assembled structures. In the case of giant vesicles, the size can be controlled in the range of 500 nm to 2.0 µm by varying the FRR in the range of $2.5 < FRR < 7.5$. At constant Q_{H_2O}, the diameter of giant vesicles decreases approximately linearly with the increase of Q_{THF} (Figure 3b). This flow-dependent variation in sizes of assemblies is opposite to the microfluidic self-assembly of molecular amphiphiles (that is, BCPs or lipids) reported previously.[11b,12a,17] The sizes of the BCP or lipid micelles increase with increasing flow rate of the fluids carrying the amphiphiles.

To achieve a better understanding of microfluidic-controlled assembly process, we simulated the microfluidic mixing between the neighboring miscible phases in a two-dimensional model using COMSOL Multiphysics 4.1. The system was modeled using the steady incompressible Navier–Stokes equation in the convection and diffusion application modes (see the detailed simulation method in the Supporting Information).[11b,18] We first studied the concentration profile of NPs in the central stream at various FRRs and fixed Q_{H_2O}. When the FRR = 18 ($Q_{H_2O} = 30$ µL min^{-1} and $Q_{THF} = 1.67$ µL min^{-1}), the narrow central stream is hydrodynamically focused, resulting in a short mixing time, t_{mix},[12c] between the water phase and the central phase containing THF and NPs (Figure 4a). The rapid depletion of the central stream quickly changes the polarity of solvent media surrounding NPs, leading to the quenching of the NP assembly to form smaller micelles (Figure 3a). With the decrease of the FRR, the central stream becomes wider and extends to the downstream channel (Figure 4b,c). The concentration of NPs remains high in the central stream, and the mixing between neighboring phases is largely determined by mutual molecular or particle diffusion in the direction normal to the streamlines. In this case, a large t_{mix} ($1.3\ s < t_{mix} < 7.4\ s$) is required to deplete the central stream gradually by forming a temporal spatial concentration gradient at the boundary. This gradient region offers a long-duration intermediate environment for the continuous growth of the assemblies into larger vesicles (Figure 3a). Figure 4e shows the concentration profile of NPs as a function of the transverse coordinate of the microchannel 4.8 mm away from the junction for various FFRs (Q_{H_2O}30 µL min^{-1}). The concentration of NPs in the central stream significantly decreased with an increase in the FRR.

In contrast to molecular amphiphiles, the significantly reduced diffusion coefficient of colloidal amphiphiles owing

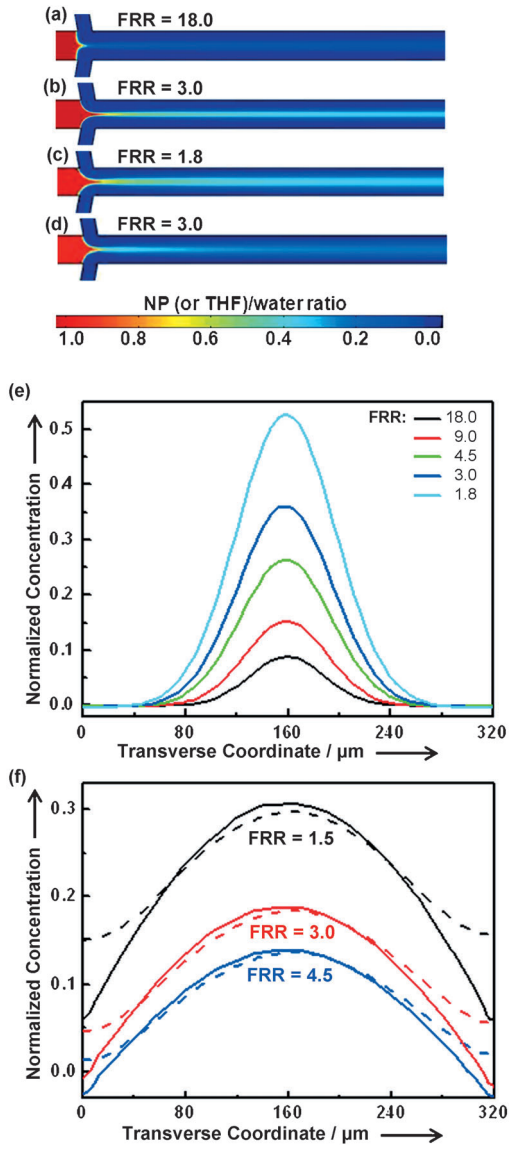

Figure 4. a–d) Simulated NP (a–c) and THF (d) concentration distribution in the focused stream at various *FRR*s. The size of NPs was set at 45 nm. $Q_{H_2O} = 30\ \mu L\,min^{-1}$. e) Simulated NP concentration profiles as a function of the transverse coordinate of the microchannel at a 4.8 mm distance away from the junction at various FRRs. $Q_{H_2O} = 30\ \mu L\,min^{-1}$. f) A comparison of the concentration profile of NPs (——) and THF (-----) as a function of the transverse coordinate of the microchannel 4.8 mm away from the junction at various FRRs. $Q_{THF} = 10\ \mu L\,min^{-1}$.

to their large size (ca. 45 nm in diameter) may influence the mutual diffusion between miscible solvents and NPs. Figures 4b,d show the concentration distribution of NPs and THF from the same system, respectively. It is clear that the suspended NPs are focused and follow the well-defined central streamline, while THF mixes more rapidly with the water phase owing to faster diffusion. This difference becomes more significant with the decrease of the FRR, owing to the dominant role of diffusive mixing at a lower FRR (Figure 4 f). Therefore, at a low FRR, NPs remain stationary in the direction vertical to the streamline while water and THF exchange more rapidly. This effect leads to a shallower region of NP concentration gradient at the stream boundaries. We presume that this mechanism explains the size decrease of the giant vesicles with the increase of Q_{THF} (or decrease of the FRR) in Figure 3b.

AuNRs are known for their strong photothermal effects in the NIR range. Upon irradiation of NIR light (700 to 1000 nm), giant vesicles can be disrupted and burst to deliver the payload owing to localized intense heating. We exposed a solution of 1.08 μm-diameter vesicles made from AuNRs to a 60 mW NIR pulsed laser beam at 800 nm. Photo-triggered rupture and fusion of vesicles were observed under an optical microscope (see the Supporting Information). It is remarkable that this disruption was complete within milliseconds of laser irradiation. After laser exposure, AuNRs were deformed to spherical AuNPs owing to the photothermally induced melting of AuNRs (Figure 5a,b; see the Supporting Information, Figure S22 for high-magnification images). The photothermally induced shape transformation of AuNRs arises from an electron–phonon relaxation process that results in the heating of free electrons of AuNRs by the absorbed photons.[19] This feature enables the application of such giant vesicles for remote-controlled release.[20] To validate this concept, the hydrophilic dye Rhodamine B (RB) was encapsulated in the vesicles during preparation. After the removal of free RB, the solution of loaded vesicles was placed in a dialysis tube and immersed in 1.5 mL of water. The release of RB was recorded by measuring the fluorescence intensity of RB in water every five minutes (see the Supporting Information for details). Without NIR laser irradiation, no obvious fluorescence intensity change in water was observed. However, when the vesicle solution was exposed to NIR laser, the RB concentration in water continuously increased with prolonged laser irradiation. As shown in Figure 5c, the increase of fluorescence intensity of RB is indicative of the release of RB from vesicles. The fluorescence increase in two independent experiments with the laser on and off clearly indicates the controlled release of RB using NIR irradiation (Figure 5d). The almost linear increase of the fluorescence intensity as a function of irradiation time implies the possibility of modulating the release dose of drugs using remote-controlled NIR switches. Compared to light-responsive vesicles based on organic chromophores,[21] AuNR vesicles are responsive to NIR light with readily tunable wavelengths by varying the aspect ratio of the NRs.[22]

In summary, we have developed a hydrodynamically controlled self-assembly method for amphiphilic NPs in MFFDs. This strategy enables both the dimension and the morphology of NP self-assemblies to be controlled. The key to manipulating this self-assembly is to balance the competition of the mixing of solvents and the assembly kinetics of AuNRs. By varying the flow rate of water and THF phases, AuNRs can assemble into a variety of nanostructures, including micelles, giant vesicles and disk-like micelles. In particular, giant vesicles were continuously generated without the use of templates through the self-assembly of amphiphilic NPs. This ability to use flow to control the organization of NPs into complex structures paves a new route to fabricating

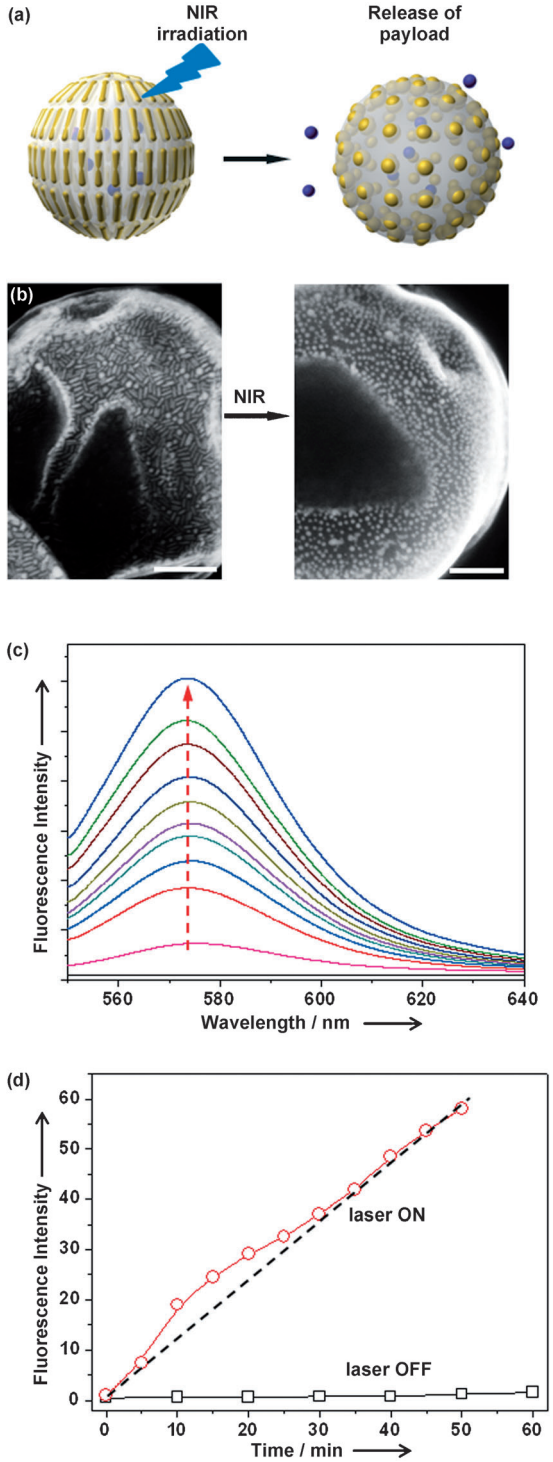

Figure 5. a) NIR-triggered release using giant vesicles. The photothermally induced shape deformation of AuNRs to spherical AuNPs creates extra spacing between AuNPs for the release of encapsulated molecules. b) SEM images of giant vesicles before and after exposed to NIR laser. The AuNRs in the vesicles deformed to spherical AuNPs upon irradiation. Scale bars are 200 nm. c) The fluorescence emission spectra of the released Rhodamine B (excitation at 540 nm) with a 5 min interval under the irradiation of 800 nm laser. d) The release profiles of Rhodamin B giant vesicles with laser on (○) and off (□).

materials and devices through NP self-assembly. We have further demonstrated the NIR-triggered burst release of encapsulated compounds from the giant vesicles. These smart vesicles may find applications in noninvasive on-command drug delivery or chemical reactions. This work will also have an impact in the areas of composites, optical resonators, sensing, catalysis, and electronics and photonics.

Received: October 19, 2012
Revised: December 15, 2012
Published online: January 30, 2013

Keywords: giant vesicles · nanoparticles · photothermal effect · plasmonic properties · self-assembly

[1] a) D. E. Discher, A. Eisenberg, *Science* **2002**, *297*, 967; b) D. A. Christian, A. W. Tian, W. G. Ellenbroek, I. Levental, K. Rajagopal, P. A. Janmey, A. J. Liu, T. Baumgart, D. E. Discher, *Nat. Mater.* **2009**, *8*, 843.

[2] a) S. H. Qin, Y. Geng, D. E. Discher, S. Yang, *Adv. Mater.* **2006**, *18*, 2905; b) J. He, X. Tong, L. Tremblay, Y. Zhao, *Macromolecules* **2009**, *42*, 7267; c) J. S. Lee, J. Feijen, *J. Controlled Release* **2012**, *161*, 473.

[3] H. Y. Lee, K. R. Tiwari, S. R. Raghavan, *Soft Matter* **2011**, *7*, 3273.

[4] a) D. A. Wilson, R. J. Nolte, J. C. van Hest, *Nat. Chem.* **2012**, *4*, 268; b) Z. Wang, M. C. van Oers, F. P. Rutjes, J. C. van Hest, *Angew. Chem.* **2012**, *124*, 10904; *Angew. Chem. Int. Ed.* **2012**, *51*, 10746.

[5] a) D. Pornpattananangkul, S. Olson, S. Aryal, M. Sartor, C.-M. Huang, K. Vecchio, L. Zhang, *ACS Nano* **2010**, *4*, 1935; b) B. D. Wang, J. Hai, Z. C. Liu, Q. Wang, Z. Y. Yang, S. H. Sun, *Angew. Chem.* **2010**, *122*, 4680; *Angew. Chem. Int. Ed.* **2010**, *49*, 4576; c) J. B. Song, L. Cheng, A. P. Liu, J. Yin, M. Kuang, H. W. Duan, *J. Am. Chem. Soc.* **2011**, *133*, 10760; d) Z. H. Nie, D. Fava, E. Kumacheva, S. Zou, G. C. Walker, M. Rubinstein, *Nat. Mater.* **2007**, *6*, 609; e) M. Grzelczak, A. Sanchez-Iglesias, H. H. Mezerji, S. Bals, J. Perez-Juste, L. M. Liz-Marzan, *Nano Lett.* **2012**, *12*, 4380; f) J. He, Y. Liu, T. Babu, Z. Wei, Z. Nie, *J. Am. Chem. Soc.* **2012**, *134*, 11342; g) M. R. Rasch, E. Rossinyol, J. L. Hueso, B. W. Goodfellow, J. Arbiol, B. A. Korgel, *Nano Lett.* **2010**, *10*, 3733; h) J. He, P. Zhang, T. Babu, Y. Liu, J. Gong, Z. Nie, *Chem. Commun.* **2013**, *49*, 576.

[6] J. B. He, P. Kanjanaboos, N. L. Frazer, A. Weis, X. M. Lin, H. M. Jaeger, *Small* **2010**, *6*, 1449.

[7] a) M. A. Horsch, Z. Zhang, S. C. Glotzer, *Nano Lett.* **2006**, *6*, 2406; b) Y. Mai, A. Eisenberg, *J Am Chem. Soc* **2010**, *132*, 10078; c) Y. Guo, S. Harirchian-Saei, C. M. S. Izumi, M. G. Moffitt, *Acs Nano* **2011**, *5*, 3309; d) M. S. Nikolic, C. Olsson, A. Salcher, A. Kornowski, A. Rank, R. Schubert, A. Fromsdorf, H. Weller, S. Forster, *Angew. Chem.* **2009**, *121*, 2790; *Angew. Chem. Int. Ed.* **2009**, *48*, 2752; e) N. A. Frey, S. Peng, K. Cheng, S. H. Sun, *Chem. Soc. Rev.* **2009**, *38*, 2532; f) K. Liu, N. N. Zhao, E. Kumacheva, *Chem. Soc. Rev.* **2011**, *40*, 656.

[8] a) M. Sauer, T. Haefele, A. Graff, C. Nardin, W. Meier, *Chem. Commun.* **2001**, 2452; b) P. Walde, K. Cosentino, H. Engel, P. Stano, *ChemBioChem* **2010**, *11*, 848.

[9] a) K. Kurihara, M. Tamura, K. Shohda, T. Toyota, K. Suzuki, T. Sugawara, *Nat. Chem.* **2011**, *3*, 775; b) A. S. Urban, T. Pfeiffer, M. Fedoruk, A. A. Lutich, J. Feldmann, *ACS Nano* **2011**, *5*, 3585; c) S. F. Fenz, K. Sengupta, *Integr. Biol.* **2012**, *4*, 982.

[10] a) H. Alkan Onyuksel, S. M. Demos, G. M. Lanza, M. J. Vonesh, M. E. Klegerman, B. J. Kane, J. Kuszak, D. D. McPherson, *J. Pharm. Sci.* **1996**, *85*, 486; b) D. V. Volodkin, A. G. Skirtach, H. Mohwald, *Angew. Chem.* **2009**, *121*, 1839; *Angew. Chem. Int. Ed.*

2009, *48*, 1807; c) T. Toyota, N. Ohguri, K. Maruyama, M. Fujinami, T. Saga, I. Aoki, *Anal. Chem.* **2012**, *84*, 3952.
[11] a) J. R. Howse, R. A. Jones, G. Battaglia, R. E. Ducker, G. J. Leggett, A. J. Ryan, *Nat. Mater.* **2009**, *8*, 507; b) A. Jahn, S. M. Stavis, J. S. Hong, W. N. Vreeland, D. L. Devoe, M. Gaitan, *ACS Nano* **2010**, *4*, 2077.
[12] a) A. Jahn, W. N. Vreeland, M. Gaitan, L. E. Locascio, *J. Am. Chem. Soc.* **2004**, *126*, 2674; b) Y. C. Tan, K. Hettiarachchi, M. Siu, Y. R. Pan, A. P. Lee, *J. Am. Chem. Soc.* **2006**, *128*, 5656; c) R. Karnik, F. Gu, P. Basto, C. Cannizzaro, L. Dean, W. Kyei-Manu, R. Langer, O. C. Farokhzad, *Nano Lett.* **2008**, *8*, 2906; d) J. C. Stachowiak, D. L. Richmond, T. H. Li, A. P. Liu, S. H. Parekh, D. A. Fletcher, *Proc. Natl. Acad. Sci. USA* **2008**, *105*, 4697; e) H. C. Shum, J. W. Kim, D. A. Weitz, *J. Am. Chem. Soc.* **2008**, *130*, 9543; f) E. Tumarkin, E. Kumacheva, *Chem. Soc. Rev.* **2009**, *38*, 2161; g) C. W. Wang, D. Sinton, M. G. Moffitt, *J. Am. Chem. Soc.* **2011**, *133*, 18853; h) P. M. Valencia, O. C. Farokhzad, R. Karnik, R. Langer, *Nat. Nanotechnol.* **2012**, *7*, 623; i) J. Liao, C. Wang, Y. Wang, F. Luo, Z. Qian, *Curr. Pharm. Des.* **2012**, *18*, 3432.
[13] A. S. Utada, E. Lorenceau, D. R. Link, P. D. Kaplan, H. A. Stone, D. A. Weitz, *Science* **2005**, *308*, 537.
[14] a) A. M. Alkilany, L. B. Thompson, S. P. Boulos, P. N. Sisco, C. J. Murphy, *Adv. Drug Delivery Rev.* **2012**, *64*, 190; b) A. Artar, A. A. Yanik, H. Altug, *Nano Lett.* **2011**, *11*, 3694; c) R. A. Alvarez-Puebla, L. M. Liz-Marzan, *Chem. Soc. Rev.* **2012**, *41*, 43.
[15] S. Nah, L. J. Li, J. T. Fourkas, *J. Phys. Chem. A* **2009**, *113*, 4416.
[16] M. Antonietti, S. Forster, *Adv. Mater.* **2003**, *15*, 1323.
[17] J. Thiele, D. Steinhauser, T. Pfohl, S. Forster, *Langmuir* **2010**, *26*, 6860.
[18] L. Wang, D. Liu, X. Wang, X. Han, *Chem. Eng. Sci.* **2012**, *81*, 157.
[19] a) L. Vigderman, E. R. Zubarev, *Langmuir* **2012**, *28*, 9034; b) B. Senyuk, J. S. Evans, P. J. Ackerman, T. Lee, P. Manna, L. Vigderman, E. R. Zubarev, J. van de Lagemaat, I. I. Smalyukh, *Nano Lett.* **2012**, *12*, 955.
[20] a) R. A. Alvarez-Puebla, E. R. Zubarev, N. A. Kotov, L. M. Liz-Marzan, *Nano Today* **2012**, *7*, 6; b) A. G. Skirtach, C. Dejugnat, D. Braun, A. S. Susha, A. L. Rogach, W. J. Parak, H. Mohwald, G. B. Sukhorukov, *Nano Lett.* **2005**, *5*, 1371; c) A. G. Skirtach, A. Munoz Javier, O. Kreft, K. Kohler, A. Piera Alberola, H. Mohwald, W. J. Parak, G. B. Sukhorukov, *Angew. Chem.* **2006**, *118*, 4728; *Angew. Chem. Int. Ed.* **2006**, *45*, 4612.
[21] Y. Zhao, *Macromolecules* **2012**, *45*, 3647.
[22] B. Nikoobakht, M. A. El-Sayed, *Chem. Mater.* **2003**, *15*, 1957.

